Dependence of the disorder-lamellar stability boundary of a melt of asymmetric wormlike *AB* diblock copolymers on the chain rigidity

Ying Jiang,* Wu-Yang Zhang, and Jeff Z. Y. Chen†

Guelph-Waterloo Physics Institute and Department of Physics and Astronomy, University of Waterloo, Waterloo, Ontario, Canada N2L 3G1

(Received 20 June 2011; revised manuscript received 31 August 2011; published 13 October 2011)

We study the disorder-order transition boundary of wormlile *AB* diblock copolymers on the basis of the wormlike chain formalism aided by a self-consistent mean-field treatment. We examine the influence of the persistency on the phase diagram and properties of the phase transition as a function of the volume fraction, Flory-Huggins parameter, and relative chain rigidity, covering a broad regime spanning from the Gaussian chain to rigid rodlike chain. On the one hand, we demonstrate that the results from a Gaussian-weight-based theory can be recovered in the long-chain limit and, on the other hand, we display that significant revisions to the phase diagram, due to the persistency effects, exist for shorter chains. A split-step numerical algorithm is designed for the computational task.

DOI: 10.1103/PhysRevE.84.041803 PACS number(s): 82.35.Jk, 36.20.Ey, 64.70.km

I. INTRODUCTION

It is now well established experimentally that a melt of *AB* diblock copolymers can phase separate into *A*-rich and *B*-rich microdomains on a nanoscale level [1,2]. As one of the most successful examples in polymer theory, the self-consistent-field theory (SCFT), which originated from the work of Edwards [3] and was developed further by Helfand and co-workers [4–7], has predicted a phase diagram in terms of essential parameters of the system, which divides into stable regions for idealized *AB* diblock copolymer micro-structures [8,9]; the SCFT approach has become an indispensable tool, coupled with various experimental approaches, to explore problems in this research area.

The basic ingredients of a SCFT for an *AB* diblock copolymer melt with an A/B volume fraction f are a statistical weight for the polymer configuration and the interaction between the *A* polymer and *B* polymer. In most theoretical developments so far, an Edwards weight has been employed as the statistical weight [3,10] and the Flory-Huggins interaction energy between *A*- and *B*-polymer components has been adopted by assuming an phenomenological Flory-Huggins parameter χ [11]. The Edwards weight, also known as a Gaussian-chain (GSC) model because it includes a quadratic Gaussian-type energy, is suitable for the description of a *flexible* polymer chain that has a total polymer contour length L and Kuhn length a [10]. According to SCFT, these ingredients yield a theory and thus the resulting phase diagram that depends on two simple parameters f and $\chi L/a$, where $L/a \gg 1$ is normally assumed in the theory, for a copolymer melt consisting of flexible *AB* diblock copolymers [8].

A much-less-explored theoretical system is the phase behavior of a *wormlike AB* diblock copolymer melt. A wormlike polymer model can be used to describe a semiflexible polymer where approximately within a segment of a persistence length λ the polymer appears rigid. In a free space, a discrete version of a wormlike chain (WLC) model was studied by Kratky and Porod [12] and a continuous version was studied by Saito, Takahashi, and Yunoki [13]. The model is appropriate for any ratio of L/λ: On the one hand, in free space it recovers GSC results in the limit of $L/\lambda \gg 1$ where $2\lambda \sim a$ can be identified and, on the other hand, it crosses over to an interesting rigid molecule limit where $L/\lambda \ll 1$. A SCFT for an *AB* diblock copolymer melt can be formulated based on a WLC model [8,14], which can be shown to contain three parameters f, $\chi L/a$, and L/a, where a is now identified with the double persistence length $a \equiv 2\lambda$. The additional L/a dependence gives rise to a theory that can be used to examine the effects of persistency, which is reflected by the finite L/a ratio, on the phase behavior of an *AB* diblock copolymer melt. This paper focuses on solving such a model to determine the stability boundary and phase behavior between a disorder phase, where *A* and *B* components are well mixed, and a lamellar phase, where the structure breaks up into *A*-rich and *B*-rich domains in a layered form Eq. (1). While we consider the full f dependence, at $f = 1/2$ our results agree well with the simplest case of symmetric *AB* diblock copolymers recently studied by Matsen [15]. The order-disorder phase separation of a wormlike *AB* diblock copolymer was also theoretically considered by Singh *et al.* [16] and Friedel *et al.* [17], who have developed somewhat different theoretical tools for these systems.

The effective Kuhn length a (or twice the persistence length λ) is a single microscopic length scale within the STY model, which is identified through the mean-square end-to-end distance in the $L/a \gg 1$ limit, $\langle R^2 \rangle = La$ [13]. Both a and the persistence length λ are different from the bare Kuhn length b, a length scale that is usually attributed to a monomer-to-monomer distance in a polymer consisting of flexible bond segments. In the more original Saito-Takahashi-Yunoki (STY) version where b was used together with a (large) bending energy penalty ϵ for two adjacent polymer bonds, $\lambda = \beta\epsilon b$ [13]. The use of the length scale λ in the STY model does not restrict us from exploring the physics of short persistent chains; the polymer can be a few bonds long measured by a short total polymer length L, where $L/\lambda \ll 1$. Both versions of the formalism, namely, maintaining a product of two parameters to explicitly indicate the presence of b, $\beta\epsilon b$, and using a single effective a (or λ) without splitting $\beta\epsilon$ from b, can be found in recent theoretical treatments.

*y35jiang@uwaterloo.ca
†jeffchen@uwaterloo.ca

A WLC-based SCFT differs from a GSC-based SCFT by the additional orientational dependence, which couples with the positional dependence usually seen in a GSC-based SCFT, in the probability distribution function for a polymer segment. A brief introduction of the theory can be found in Sec. II. The orientational dependence is essential for dealing with wormlike systems where orientational properties are the major concern, such as in studying the thermodynamics of polymer liquid crystals [18–21] and spatially inhomogeneous polymer liquid-crystal systems [22–29]. The orientational dependence is also required to render the correct physical properties for spatially inhomogeneous wormlike polymer problems where the positional dependence is the main concern, such as the system examined in this work, phase separation of AB bulk polymers [30], the wormlike chain in confinement [31–34], the wormlike polymer adsorption problem [35,36], and the wormlike polymer brush problem [37].

Computationally, the spatial and orientational variables in the WLC probability function need to be simultaneously represented in numerical approaches, which can be summarized into the following categories. (i) Both orientational and spatial dependences are treated by finite-difference schemes [28]. In numerical results, to achieve the same precision as those from (ii) and (iii) below, an extremely high computational resource is required. (ii) The orientational dependence is treated by an expansion in terms of the spherical harmonics and the spatial dependence by a finite-difference scheme [24,25,29]. For a sharp boundary condition and interface, this method only works successfully with a high resolution on the spatial variable, resulting in a high computational demand. The intermediate and strong segregation regimes of the current problem correspond to a relatively sharp interface [38]. (iii) Both orientational and spatial dependences are treated by combinatorial orthonormal eigenfunctions [15]. Because of the smoothness of the eigenfunctions used in this approach, the number of eigenfunctions containing the spatial variables can be significantly lower than the number of divisions in the spatial-variable space and thus is much less computationally demanding than the two preceding methods. For the current problem, we adopt an extended version of (iii) in which spherical harmonic functions and Fourier bases are used as eigenfunctions of the orientational and spatial variables.

A key quality of an efficient and accurate numerical algorithm for solving the resulting modified diffusion equation from a WLC-based SCFT relies on a careful design to treat the timelike variable together with the orientational and spatial variables. In this paper a numerical strategy in the spirit of the split-step algorithm is developed [39,40], which amounts to an error corresponding to a third order in the step length of the timelike variable with no restriction on the precision of representing the orientational and spatial variables. This can be compared with the Crank-Nicolson [41] method advanced previously, which contains a numerical error of the second order in the step length of the timelike variable and has a concurrent requirement on the precision of the orientational and spatial variables. In addition, a direct forward time-difference scheme would introduce an error of the same order as the step length in the time variable and thus requires very small divisions [25,28]. The details of our implementation of the split-step algorithm can be found in Sec. II B.

Our focus in this paper is a thorough study to demonstrate the effects of persistency on the disorder-lamella transition, which contains a one-dimensional spatial variation. The phase diagram of semiflexible AB diblock copolymers of Gaussian chains displays a wealth of other order structures as well, especially in the $f \neq 1/2$ regime [42]. A complete study of the phase diagram of AB diblock copolymers, including cubic, hexagonal, and gyroid structures, requires computation of the formalism in this paper in two- and three-dimensional space, which is a computational challenge that currently cannot be easily attacked.

The main numerical results are given and discussed in Sec. III; readers who do not wish to review the self-consistent mean-field treatment and numerical approaches can directly skip to this section.

II. THEORY

In the first part of this section we outline the self-consistent-field theory used to treat the current problem, on the basis of the Saito-Takahashi-Yunoki model [13] for the description of a wormlike chain in an external field [14]. While the general theoretical development can be found elsewhere [14], we pay attention to the particular form used for the current system. In the second part of this section we discuss the computational methods used to solve the differential equation yielded by the self-consistent-field theory.

A. Self-consistent-field theory

Consider a polymer melt of n undistinguishable AB diblock copolymer chains occupying a volume V of an incompressible system, each having a total contour length L and a bare persistence length λ. The diblock copolymer is made of a segment of A polymer of length fL connecting to a segment of B polymer of length $(1-f)L$. The parameter λ is assumed to be the same for both A and B segments, though the theoretical framework below can also be used for two segments having different persistent lengths [25,26,28]. The interaction energy per segment is assumed to have the Flory-Huggins form

$$\beta F_{\mathrm{FH}} = \chi \int d\mathbf{r}\phi_A(\mathbf{r})\phi_B(\mathbf{r}), \tag{1}$$

where $\phi_A(\mathbf{r})$ and $\phi_B(\mathbf{r})$ are the volume fractions at a point with the coordinate $\mathbf{r}$. One basic assumption is that these two functions represent the overall volume fraction variations, already averaged over the angular dependence (see below). This assumption was also used previously by Morse and Fredrickson [30] and Matsen [15] for wormlike polymers.

Of central concern in the self-consistent-field theory is the calculation of the propagator $q(\mathbf{r},\mathbf{u},s)$, which represents the probability of finding a polymer segment of length sL (starting from the A terminus) with the ending monomer located at $\mathbf{r}$ and the ending segment pointing at the orientation specified by a unit vector $\mathbf{u}$. The arc variable s is a label for the path location of a polymer; our convention is that $s=0$ represents the A terminus and $s=1$ the B terminus. The partition function of a single chain Q can be calculated from

$$Q = (1/4\pi V)\int d\mathbf{r}\, d\mathbf{u}\, q(\mathbf{r},\mathbf{u},1), \tag{2}$$

where a prefactor $1/4\pi V$ has been introduced to normalize the integral. The volume fractions for components A and B can be calculated from

$$\phi_A(\mathbf{r}) = \frac{1}{4\pi Q}\int d\mathbf{u}\int_0^f ds\, q(\mathbf{r},\mathbf{u},s)q^*(\mathbf{r},\mathbf{u},s), \quad (3)$$

$$\phi_B(\mathbf{r}) = \frac{1}{4\pi Q}\int d\mathbf{u}\int_f^1 ds\, q(\mathbf{r},\mathbf{u},s)q^*(\mathbf{r},\mathbf{u},s), \quad (4)$$

where a complementary propagator $q^*(\mathbf{r},\mathbf{u},s)$ has been used. This propagator represents the probability of finding a polymer segment of length $(1-s)L$ (starting from the B terminus) with the ending monomer located at $\mathbf{r}$ and the ending segment pointing at the orientation specified by a unit vector $-\mathbf{u}$.

There are two ways of writing down the propagator in terms of the STY model in an external field $\omega(\mathbf{r};\tau)$. The integral form of the calculation of $q(\mathbf{r},\mathbf{u},s)$ is given by

$$q(\mathbf{r},\mathbf{u},s) = \int \mathcal{D}\mathbf{r}\, P[\mathbf{r};0,s]\delta(\mathbf{r}-\mathbf{r}(s))\delta(\mathbf{u}-\mathbf{u}(s)) \times \exp\left[-\int_0^s d\tau\, \omega(\mathbf{r};\tau)\right], \quad (5)$$

with the statistical weight [13]

$$P[\mathbf{r};s_1,s_2] \propto \delta(1-|\mathbf{u}(s)|)\exp\left[-\frac{\lambda}{2L}\int_{s_1}^{s_2} ds\left|\frac{d}{ds}\mathbf{u}(s)\right|^2\right]. \quad (6)$$

The vector representing the tangent direction at s is defined as $\mathbf{u}(s) \equiv (1/L)[d\mathbf{r}(s)/ds]$, which is constrained to be a unit vector by the delta function in Eq. (6). For the external field in the large square bracket of Eq. (5), we have

$$\omega(\mathbf{r};s) = \begin{cases} \omega_A(\mathbf{r}) \equiv \omega_+(\mathbf{r}) - \omega_-(\mathbf{r}) & \text{if} \quad 0 \leqslant s \leqslant f, \\ \omega_B(\mathbf{r}) \equiv \omega_+(\mathbf{r}) + \omega_-(\mathbf{r}) & \text{if} \quad f < s \leqslant 1, \end{cases}$$

where $\omega_A(\mathbf{r})$ and $\omega_B(\mathbf{r})$ are the external fields acting on the A and B components, respectively. The axillary fields $\omega_\pm(\mathbf{r})$ are defined above for later convenience. The results from the calculation of the propagator depend on these two fields. Note that if we set these fields equal to zero, we return to the original STY problem [13], where one can show that the bare persistence length λ is related to the Kuhn length a by

$$a = 2\lambda, \quad (7)$$

from the definition of the mean-square end-to-end distance of a long wormlike chain. In the rest of this paper, we use a directly instead of λ, which allows us to make a comparison with the theory based on a Gaussian-chain model, with an understanding of the above connection.

The differential-equation form is an equivalent way of writing down the propagator-field relationship [8]

$$\frac{\partial}{\partial s}q(\mathbf{r},\mathbf{u},s) = \left[\frac{L}{a}\nabla_{\mathbf{u}}^2 - L\mathbf{u}\cdot\nabla_{\mathbf{r}} - \omega(\mathbf{r};s)\right]q(\mathbf{r},\mathbf{u},s). \quad (8)$$

The propagator can be determined by solving this modified diffusion equation from a given external field ω, subject to the initial condition $q(\mathbf{r},\mathbf{u},0) = 1$. Since the two termini of the AB copolymer are distinct, we need to solve the equation

$$\frac{\partial}{\partial s}q^*(\mathbf{r},\mathbf{u},s) = \left[-\frac{L}{a}\nabla_{\mathbf{u}}^2 - L\mathbf{u}\cdot\nabla_{\mathbf{r}} + \omega(\mathbf{r};s)\right]q^*(\mathbf{r},\mathbf{u},s) \quad (9)$$

separately from Eq. (8), with the initial condition $q^*(\mathbf{r},\mathbf{u},1) = 1$. These modified diffusion equations (8) and (9) are usually computed numerically to obtain the properties of the system instead of the direct evaluation of the propagators from the integral in Eq. (5).

For the current system we can formally express the free-energy difference per chain (in units of $1/\beta \equiv k_BT$) in terms of $\omega_\pm(\mathbf{r})$ [43],

$$\beta\Delta F \equiv \beta F - \beta F_0 = -\ln Q + \frac{1}{V}\int d\mathbf{r}\left[\frac{\omega_-^2(\mathbf{r})}{(\chi L/a)} + (2f-1)\omega_-(\mathbf{r}) - \omega_+(\mathbf{r})\right], \quad (10)$$

where the free energy of the disordered phase $F_0 = (\chi L/a)f(1-f)$ is used as a reference. The functional minimization of the free energy with respect to the two fields $\omega_-(\mathbf{r})$ and $\omega_+(\mathbf{r})$ gives rise to two equations

$$\phi_B(\mathbf{r}) - \phi_A(\mathbf{r}) + \left[\frac{2}{(\chi L/a)}\omega_-(\mathbf{r}) + (2f-1)\right] = 0 \quad (11)$$

and

$$\phi_A(\mathbf{r}) + \phi_B(\mathbf{r}) - 1 = 0. \quad (12)$$

These equations close the self-consistency loop for the numerical calculation carried out in this work; in total, Eqs. (8), (9), (3), (4), (11), and (12) are solved self-consistently for a given set of parameters f, L/a, and $\chi L/a$. The free energy can then be obtained from the calculation on the right-hand side of Eq. (10).

B. Numerical approach

The computational strategy used in this work depends on iterations that correct a previous estimate. Initially, an approximation for the external fields $\omega_-(\mathbf{r})$ and $\omega_+(\mathbf{r})$ is made that can be used to obtain $q(\mathbf{r},\mathbf{u},s)$ and $q^*(\mathbf{r},\mathbf{u},s)$ through solving Eqs. (8) and (9) numerically for the entire $0 \leqslant s \leqslant 1$ range. Then the density profiles for components A and B can be computed straightforwardly from Eqs. (3) and (4). As a naive approach the next step would be to calculate an improved approximation for the external fields by directly requiring that Eqs. (11) and (12) are satisfied. However, this step is not always numerically stable and thus is not used in the actually numerical implementation. Following the work done by Fredrickson *et al.* [43], instead of taking Eqs. (11) and (12) in their original forms, we use the effective relaxation equations

$$\frac{\partial}{\partial t}\omega_-(\mathbf{r},t) = -\xi_-\left\{\phi_B(\mathbf{r},t) - \phi_A(\mathbf{r},t) + \left[\frac{2}{(\chi L/a)}\omega_-(\mathbf{r},t) + (2f-1)\right]\right\}, \quad (13)$$

$$\frac{\partial}{\partial t}\omega_+(\mathbf{r},t) = \xi_+[\phi_A(\mathbf{r},t) + \phi_B(\mathbf{r},t) - 1], \quad (14)$$

in a forward-difference scheme for t with a step length Δt. The coefficients $\Delta t\xi_-$ and $\Delta t\xi_+$ control the relaxation rate of the convergence in solving Eqs. (13) and (14). Large relaxation coefficients yield a faster search for the equilibrium solution,

but are also accompanied by an undesirable instability. We found in our calculation that for the current system an appropriate range is $0.2 \leqslant \Delta t\xi_{-}, \Delta t\xi_{+} \leqslant 0.6$. The fields $\omega_{-}(\mathbf{r},t)$ and $\omega_{+}(\mathbf{r},t)$, which are calculated from the relaxation method, update once after a full calculation of q and q^{*} is done; then they are used as a new guess in Eqs. (8) and (9) for the starting point of a new iteration.

Within this computational strategy, a crucial step is accurately and efficiently carrying out the solution to Eqs. (8) and (9). Formally, an exact expression can be obtained for Eq. (8),

$$q(\mathbf{r},\mathbf{u},s+\Delta s) = \exp\left[\Delta s\left(\mathcal{L}^{\nabla_{\mathbf{u}}^2} + \mathcal{L}^{\nabla_{\mathbf{r}}} + \mathcal{L}^{\omega}\right)\right] q(\mathbf{r},\mathbf{u},s), \quad (15)$$

which is valid for any size of Δs. The three operators appearing in the above expression are $\mathcal{L}^{\nabla_{\mathbf{u}}^2} \equiv (L/a)\nabla_{\mathbf{u}}^2$, $\mathcal{L}^{\nabla_{\mathbf{r}}} \equiv -L\mathbf{u}\cdot\nabla_{\mathbf{r}}$, and $\mathcal{L}^{\omega} \equiv -\omega_j(\mathbf{r})$, $(j = A, B)$. Performing the Baker-Campbell-Hausdorff operator identity twice [44],

$$\begin{aligned} & e^{\Delta s\mathcal{L}^{\omega}} e^{\Delta s\mathcal{L}^{\nabla_{\mathbf{r}}}} e^{\Delta s\mathcal{L}^{\nabla_{\mathbf{u}}^2}} \\ & = \exp\left\{\Delta s\left(\mathcal{L}^{\omega} + \mathcal{L}^{\nabla_{\mathbf{r}}} + \mathcal{L}^{\nabla_{\mathbf{u}}^2}\right) + \frac{\Delta s^2}{2}\left(\left[\mathcal{L}^{\omega},\mathcal{L}^{\nabla_{\mathbf{r}}}\right]\right.\right. \\ & \left.\left. + \left[\mathcal{L}^{\omega},\mathcal{L}^{\nabla_{\mathbf{u}}^2}\right] + \left[\mathcal{L}^{\nabla_{\mathbf{r}}},\mathcal{L}^{\nabla_{\mathbf{u}}^2}\right]\right) + O(\Delta s^3)\right\}, \end{aligned} \quad (16)$$

where $[\mathcal{L}^{\omega},\mathcal{L}^{\nabla_{\mathbf{r}}}] \equiv \mathcal{L}^{\omega}\mathcal{L}^{\nabla_{\mathbf{r}}} - \mathcal{L}^{\nabla_{\mathbf{r}}}\mathcal{L}^{\omega}$ represents the operator commutator, we can obtain the solution to the propagator

$$\begin{aligned} q(\mathbf{r},\mathbf{u},s+\Delta s) = {} & e^{\Delta s\mathcal{L}^{\omega}/2} e^{\Delta s\mathcal{L}^{\nabla_{\mathbf{r}}}/2} e^{\Delta s\mathcal{L}^{\nabla_{\mathbf{u}}^2}} e^{\Delta s\mathcal{L}^{\nabla_{\mathbf{r}}}/2} \\ & \times e^{\Delta s\mathcal{L}^{\omega}/2} q(\mathbf{r},\mathbf{u},s) + O(\Delta s^3). \end{aligned} \quad (17)$$

The advantage of using Eq. (17) is that for a small Δs, terms of order Δs^2 exactly cancel out and the error only amounts to an order of Δs^3 and higher. This can be compared with the Crank-Nicolson method, which is commonly used in solving modified diffusion equations such as those in our previous works [29,37], where a numerical error of order Δs^2 is introduced [41]. We also note that some forward-difference-based algorithms were previously used for the calculation of the propagator [28,45].

To apply this method further, we need to deal with the $\mathcal{L}$ operators. The spherical harmonics and Fourier bases are the eigenfunctions of the operators $\mathcal{L}^{\nabla_{\mathbf{u}}^2}$ and $\mathcal{L}^{\nabla_{\mathbf{r}}}$, respectively. As long as the transformations connecting the variables $\mathbf{u}$ and $\mathbf{r}$ and the expansion coefficients of spherical harmonics and Fourier functions are provided, the split-step algorithm is efficient for carrying out the calculations associated with the exponential operations [39,40]; the method is known to be unconditional stable and highly accurate, which means that fewer expansion coefficients and a relatively large step length Δs can be taken in the actual calculation. A similar algorithm was constructed by Tzeremes *et al.* [46] to solve the modified diffusion equation previously deduced from a Gaussian-chain model. This approach has multiple advantages over a finite-difference scheme, which requires a more careful division of the variable space to match the correct order in Δs in order to avoid numerical divergence.

Further simplifications can be made for the present study of a lamellar phase, where only one spatial variable x and one orientational variable θ (between the axis x and orientational vector $\mathbf{u}$ shown in Fig. 1) are considered. For a function of x

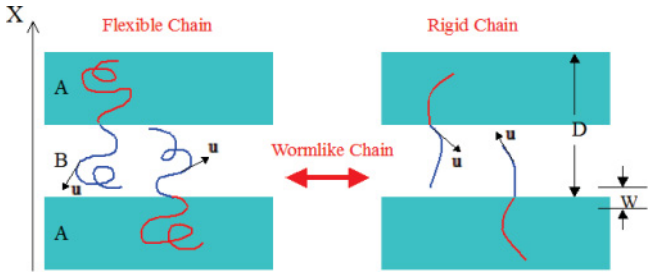

FIG. 1. (Color online) Sketches of a lamellar morphology for the AB diblock copolymers: Shown on the left-hand side are flexible polymers that can be described by the Gaussian-chain formalism and the long-chain limit of the current wormlike-chain formalism and on the right-hand side is a rigid-chain limit that is also covered in this work. The wormlike-chain formalism leads to a smooth crossover between these two limits.

and the associated Fourier transformation k, we can define the Fourier transform $\hat{F}$ and the inverse Fourier transform $\hat{F}^{-1}$. For a function of θ and its Legendre function of rank l, we can define the Legendre transform $\hat{S}$ and the synthesis of the Legendre transform $\hat{S}^{-1}$. We can then write

$$\begin{aligned} & q(x,\theta,s+\Delta s) \\ & \approx e^{-\Delta s\omega_j(x)/2}\hat{F}^{-1}\{e^{-i\Delta sk\cos\theta/2}\hat{F}[\hat{S}^{-1}(e^{-\Delta s(L/a)l(l+1)} \\ & \times\hat{S}(\hat{F}^{-1}\{e^{-i\Delta sk\cos\theta/2}\hat{F}[e^{-\Delta s\omega_j(x)/2}q(x,\theta,s)]\}))]\}. \end{aligned} \quad (18)$$

The Fourier bases used for the lamellar phase can be characterized by a discrete set

$$k_m = 2\pi m/D, \quad (19)$$

where m is an integer and D is the lamellar domain size considered in Fig. 1. The same resolution for x as the one used by Matsen [15] was adopted in this work. In practice, these transformations are performed based on well-established numerical procedures such as those given in Ref. [41]. The truncated expansion index l and the corresponding number of equally divided grids on polar angle θ are appropriately adjusted according to the convergence criteria $\max|\omega_{\pm}^{\text{new}}(x) - \omega_{\pm}^{\text{old}}(x)| < 10^{-4}$. This way the free energy produced depends on the domain size D; an additional computational task is to search for the minimum free energy as a function of D [47]. The results reported below correspond to an optimal D after such minimization.

III. RESULTS AND DISCUSSION

This work considers the influence of the chain persistency on the physical properties from the disorder-lamellar stability analysis. As discussed in the Introduction and shown exactly in Sec. II, three independent parameters emerge to be important: the scaled Flory-Huggins interaction parameter $\chi L/a$, the volume fraction of the A component f, and the effective number of Kuhn segments in a wormlike chain L/a. Note that f and $\chi L/a$ are the same combination of parameters as in the Gaussian-chain theory for the lamellar phase; in the latter case the parameter L/a is normally related to the number of monomers in a typical theory and is take to be a large number [8].

In particular, we discuss below the numerical results from our self-consistent-field theory in terms of a stability diagram where the disorder-lamellar (DL) boundary divides the stability regions of the disorder and lamellar states, determined from an examination of the free energy $F = F(f, L/a, \chi L/a)$. We also discuss the properties of the lamellar domain size $D/a \equiv \tilde{D}(f, L/a, \chi L/a)$, which was optimized to minimize the lamellar free energy per domain. We further discuss an interfacial width

$$W = \left[\max\left|\frac{d}{dx}\phi_A(x)\right|\right]^{-1}, \tag{20}$$

where the function max takes the maximum value of its argument. The rescaled interfacial width $W/a \equiv \tilde{W}(f, L/a, \chi L/a)$ is a function of f, L/a, and $\chi L/a$ as well.

A. Flexible limit: $L/a \gg 1$

Our first concern is whether the DL stability boundary determined by the current WLC model would recover what we have already known from the classical random-phase approximation (RPA) [48] of a Gaussian-chain model in the limit of $L/a \gg 1$. As shown in Fig. 2, the DL boundaries (represented by symbols) determined from the WLC model for various values of L/a have a reasonable trend to asymptotically approach the solid curve, which was obtained from a weak-inhomogeneity expansion based on the assumption of a Gaussian-type statistical weight of a polymer configuration [48]; the $L/a = 100$ curve (squares in Fig. 2) from our calculation even substantially overlaps with the RPA result.

In many wormlike-chain systems, the recovery of the Gaussian-chain result is *not* a trivial notion even in the limit of $L/a \gg 1$ and needs to be carefully justified; the magnitude of

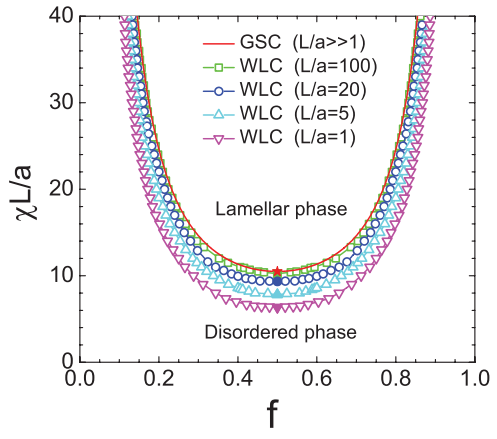

FIG. 2. (Color online) Numerical results for the disorder-lamellar stability boundary based on a wormlike-chain (WLC) model for AB diblock copolymers for several selected values of L/a: 100, 20, 5, and 1, represented by squares, circles, triangles, and inverted triangles, respectively. These results can be compared to the stability boundary obtained from the calculation based on a random-phase approximation of a Gaussian-chain (GSC) model, which is shown by the solid curve. All boundaries have the characteristics of a first-order phase transition, terminating at a second-order point represented by the solid points at $f = 1/2$.

a/W, where W characterizes a typical length scale on which the density profile varies drastically, determines whether or not the Gaussian-chain limit is approached [34,36]. In the current model, the spatial variation of the density profile is reflected in the main equations (8) and (9) by the derivative term $L\mathbf{u}\cdot\nabla_{\mathbf{r}} = (L/a)(a/W)\cos\theta\, d/d\tilde{x}$, where $\tilde{x} \equiv x/W$. While the L/a prefactor is comparable to the magnitude of the first term in Eqs. (8) and (9), the magnitude of a/W is responsible for whether or not a Gaussian-weight-based SCFT can be recovered from a WLC-based SCFT. Indeed, taking a simultaneous expansion of the propagator in terms of the Legendre functions and powers of small a/W, we can show that in the lamellar phase

$$\chi \sim (a/W)^2$$

and Eqs. (8) and (9) exactly recover the counterpart diffusion equation in a Gaussian theory for $L/a \gg 1$ [49].

This can be interpreted in a physical picture. In the flexible polymer limit $L/a \gg 1$, each wormlike polymer has approximately the size of the Gaussian gyration radius in a disorder phase $(aL)^{1/2}$. Approaching the DL instability boundary from the disorder side, once the phase separation takes place in the form of a continuous or weak first-order transition, both the domain size D and interfacial width W are on the order of $(aL)^{1/2}$. This guarantees that the ratio a/W is approximately $a/W \sim (a/L)^{1/2}$, which is small in the limit of $a/L \ll 1$. For comparison, because $\chi L/a$ represents the immiscibility interaction between polymer segments A and B, we expect that phase separation takes place when $\chi L/a \sim 1$ or $\chi \sim a/L$; hence the estimate $\chi \sim (a/W)^2$ is physically justifiable. Numerically, Figs. 3(b) and 3(c) demonstrate how both $D/(aL)^{1/2}$ and $W/(aL)^{1/2}$ in the lamellar state approach an L/a-independent limit as L/a increases, which are results from wormlike-polymer-based SCFT.

Because the DL stability boundary is determined from the free energy, the approaching of the asymptotic GSC result in Fig. 2 is the direct consequence of the asymptotic behavior of the free energy, displayed in Fig. 3(a). For a specified value of f and $\chi L/a$, as a function of L/a, an L/a-independent asymptotic limit can be viewed in these plots when $L/a \gg 1$.

Within a GSC model, Leibler showed that the DL stability boundary has the characteristics of a second-order phase transition at $f = 0.5$ and a first-order phase transition for $f \neq 0.5$ [48]. These properties can be directly examined in terms of the lamellar free-energy difference $\Delta F = F - F_0$, where F_0 is the free energy of the disordered phase, and the inverse-scaled interfacial width $(aL)^{1/2}/W$ as an order parameter that has a value of $(aL)^{1/2}/W = 0$ in the disorder phase. As a function of $(\chi - \chi_{\mathrm{DL}})L/a$ for a given value of f, where χ_{DL} is the value at the DL transition boundary, ΔF is negative inside the lamellar region and displays quadratic behavior near the transition point for $f = 0.5$ and a straight line near the transition point for $f \neq 0.5$, according to the mean-field understanding of the phase-transition theory. The solid curve in the top panel of Fig. 4(a) and the solid line in the top panel of Fig. 5(a) are examples of these critical behaviors. As a function of the same variable, for $f = 1/2$ where the transition is second order, the order parameter in the lamellar phase is expected to display a power law with an critical exponent of $1/2$, hence the square order parameter showing a

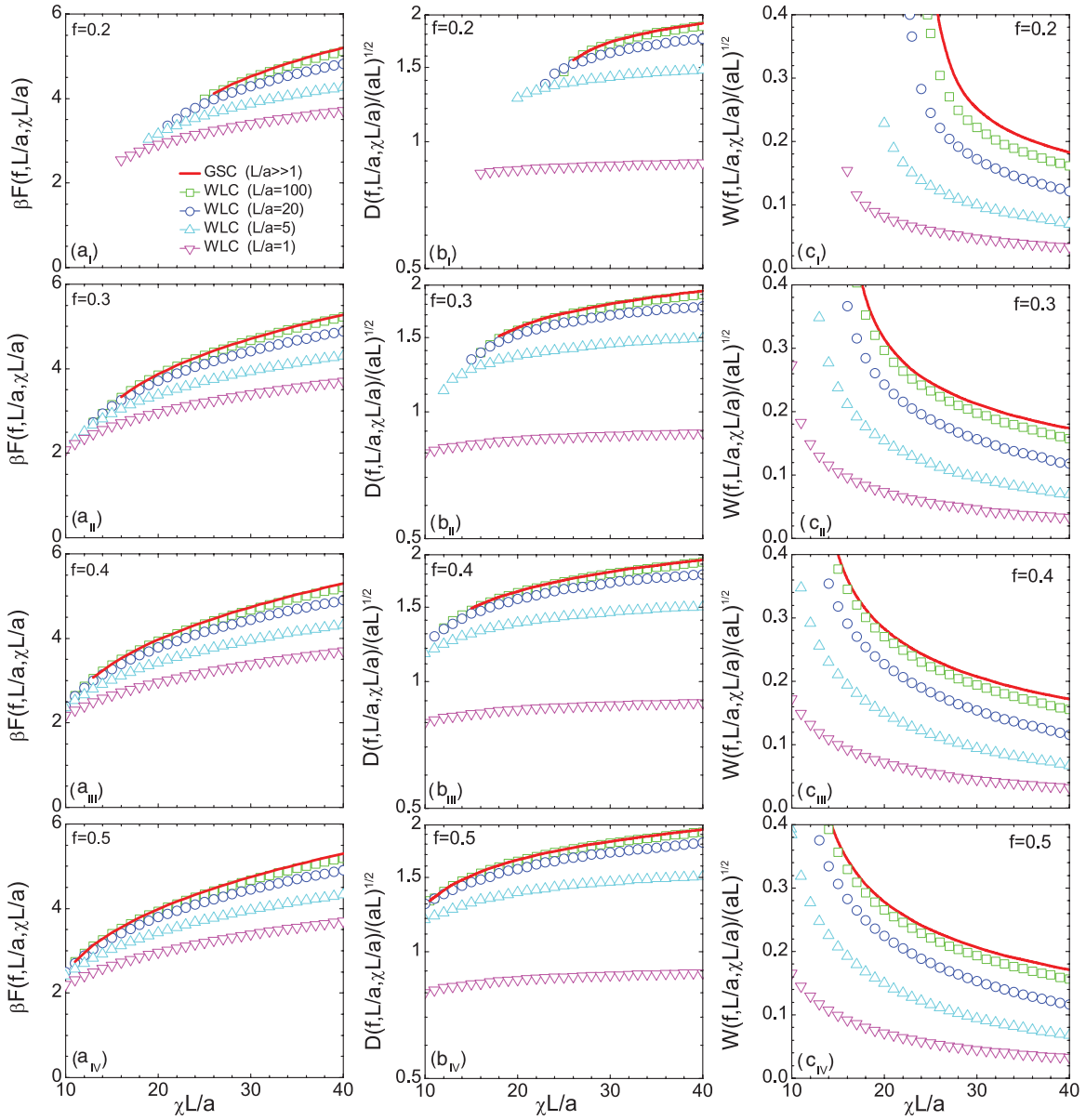

FIG. 3. (Color online) (a) Lamellar free energy $F(f,L/a,\chi L/a)$, (b) reduced domain size $D(f,L/a,\chi L/a)/(aL)^{1/2}$, and (c) reduced interfacial width $W(f,L/a,\chi L/a)/(aL)^{1/2}$ as functions of the reduced Flory-Huggins parameter $\chi L/a$ for volume fraction (I) $f = 0.2$, (II) $f = 0.3$, (III) $f = 0.4$, and (IV) $f = 0.5$, computed from the wormlike-chain formalism. In these plots, chain sizes $L/a = 100$, 20, 5, and 1 are represented by squares, circles, triangles, and inverted triangles, respectively. The results from a GSC formalism, valid for $L/a \gg 1$, are also plotted as the solid curves.

straight line [solid line in the bottom panel of Fig. 4(a)]; for $f \neq 1/2$ where the transition is first order, the order parameter abruptly jumps to zero when the system goes through the transition point from the lamellar phase [solid line in the bottom panel of Fig. 5(a)]. The long-chain results yielded by the WLC model, displayed in these plots by squares for $L/a = 100$, fully agree with these characteristics near the transitions.

B. Intermediate region: $L/a \sim 1$

Moving away from the extremely large L/a region, we start to see the effects of persistency in the stability diagram (Fig. 2). For L/a as large as $L/a = 20$, the stability boundary already moves significantly below the GSC result. The DL stability boundaries deviate even more remarkably from the RPA result in the smaller $L/a = 5$ and 1 cases. According to this diagram, we conclude that one of the main effects of the chain persistency is broadening of the lamellar stability region accompanied by a lower transition $\chi_{\rm DL}L/a$. Physically, a more rigid polymer chain loses less conformational entropy in a stretched conformation in comparison with its Gaussian counterpart of the same length. One consequence in our system is that persistency makes it easier for the system to phase separate (which decreases a polymer's entropy) for the same value of the $\chi L/a$ parameter. This is the underlying reason for the broadening of the lamellar stability region in Fig. 2, which is similar to the observation by Friedel *et al.* [17].

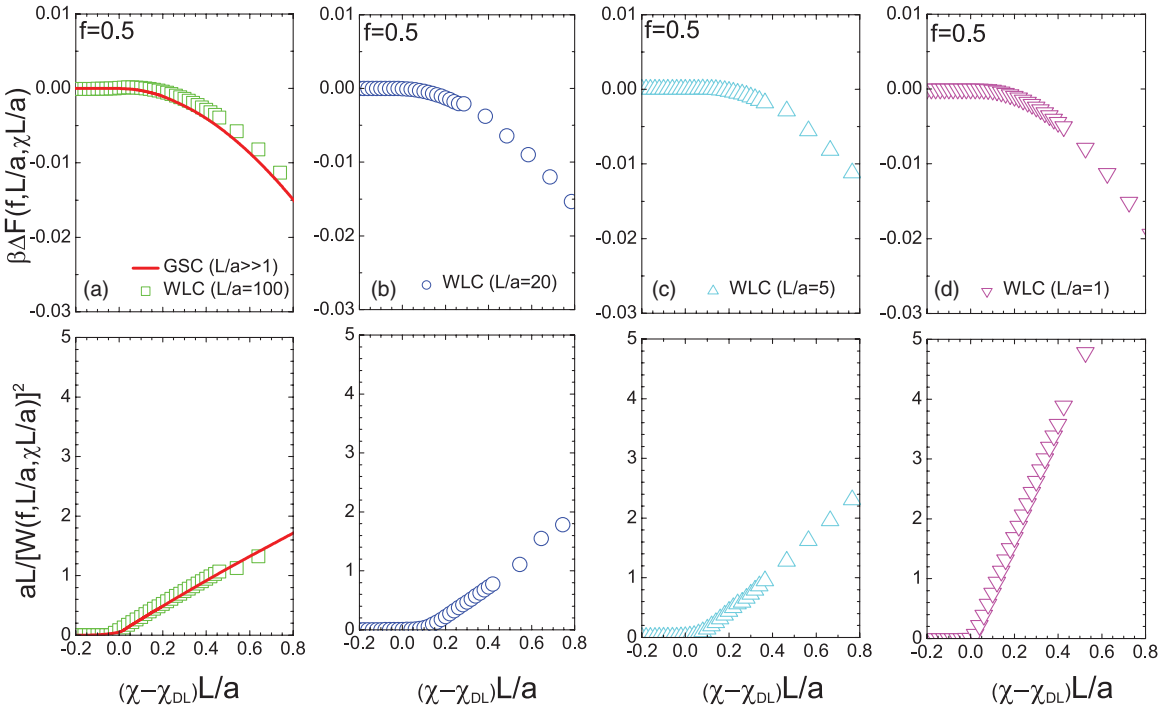

FIG. 4. (Color online) Symmetric AB diblock copolymers ($f = 1/2$): numerical results for the lamellar free-energy difference (top panels) and square order parameter (bottom panels) as functions of $(\chi - \chi_{DL})L/a$, where $\chi_{DL}L/a$ is the critical point specified by a solid symbol in Fig. 2. We consider the properties for a GSC model for $L/a \gg 1$ [solid curve in (a)] and a WLC model for $L/a = 100$ (squares), 20 (circles), 5 (triangles), and 1 (inverted triangles).

Going from the flexible chain limit (large L/a) to a more rigid molecule (small L/a), the typical domain size of the lamella crosses over from $D \sim (aL)^{1/2}$ (Gaussian coil size) to $D \sim L$ (rod size); similarly, this happens to a typical interface width that crosses over from $W \sim (aL)^{1/2}$ to L as well. In the intermediate region, we expect to see that both D and W deviate significantly from these asymptotic behaviors. The crossover can be viewed from the numerical examples shown in Fig. 6, where we see that both D/a and W/a scale as $(L/a)^{1/2}$ in the large L/a limit and as L/a in the small L/a limit.

In terms of a phase transition, the phase boundary at $f = 1/2$ is second order according to the GSC model [48]; this second-order nature is confirmed by our calculation of the WLC model, which is now valid for any ratio of L/a, even in the small L/a region. The numerical evidence can be found in four plots ($L/a = 100$, 20, 5, and 1) of Fig. 4 where the order parameter $(aL)^{1/2}/W$ can be seen to always vary continuously across the transition point χ_{DL}. In all these cases, our data also demonstrate that a mean-field critical exponent of 1/2 is followed by the order parameter in a lamellar phase near the transition point (hence an exponent of 1 for the square order parameter in the figure). Furthermore, in the top panels of these plots, the lamellar free-energy difference can be seen to connect to $\Delta F = 0$ in the disorder phase by a smoothly varying slope.

Figure 5 shows the free-energy difference and order parameter for an asymmetric case $f = 0.2$, which demonstrates a different behavior. The order parameter $(aL)^{1/2}/W$ goes through a finite jump and the free-energy difference displays a straight line approaching the transition point χ_{DL} from the lamellar phase. These are characteristics of a first-order transition, valid for all other values of f (as long as $f \neq 1/2$) as well (figures not shown). The first-order jump in the order parameter weakens and finally vanishes as f approaches 1/2. That is, along all DL stability boundaries described in Fig. 2, only symmetric WLC AB diblock copolymers ($f = 1/2$) have a second-order transition (shown by solid symbols in the figure).

C. Remarks

For the case of $f = 1/2$ (symmetric lamellar morphology), our WLC results are in full agreement with those considered by Matsen, after making the identification of his κ with 1/2 [15]. In Fig. 7, using solid curves we replotted Matsen's DL stability boundary $\chi_{DL}(f = 1/2, L/a)L/a$ and lamellar domain size $D(f = 1/2, L/a, \chi_{DL}L/a)/(aL)^{1/2}$ by reading off data from the figures of his publication. Overlapping the curves are our results for various values of L/a. One interesting limit is $L/a \to 0$, the limit of a rigid rod chain. From our data in the figure we see that $\chi_{DL}(f = 1/2, L/a)L/a$ asymptotically approaches 6.18 ± 0.02, which agrees with Matsen's estimate of 6.135 [15] within the numerical error; however, both are far lower than the values of 8.30 suggested by Singh *et al.* [16] and 7.55 by Friedel *et al.* [17].

The WLC stability diagram presented in Fig. 2 is based on the comparison of the free energy of two possible states occurring in an AB diblock copolymer system: disorder and lamellar. We use this example to demonstrate the importance

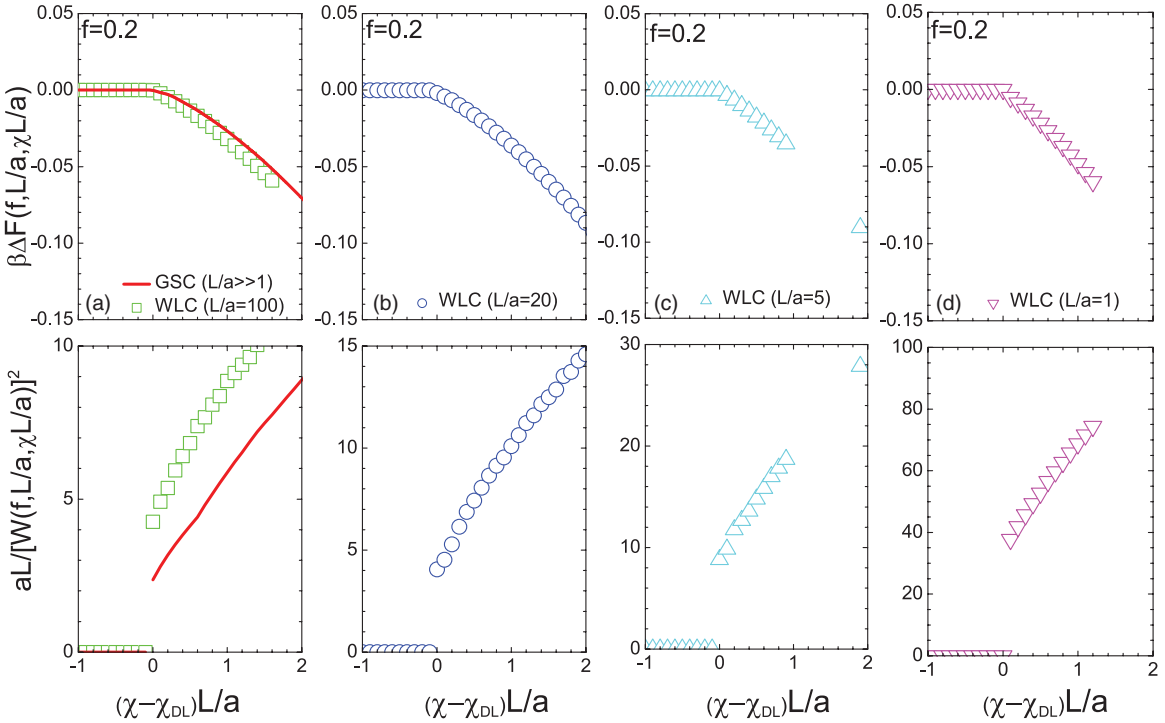

FIG. 5. (Color online) Example of asymmetric AB diblock copolymers ($f = 0.2$): numerical results for the lamellar free-energy difference (top panels) and square order parameter (lower panels) as functions of $(\chi - \chi_{\rm DL})L/a$, where $\chi_{\rm DL}L/a$ is the first-order transition point. We consider the properties for a GSC model for $L/a \gg 1$ [solid curve in (a)] and a WLC model for $L/a = 100$ (squares), 20 (circles), 5 (triangles), and 1 (inverted triangles).

of the influence of chain persistency in determining the free energy and hence the phase diagram of AB diblock copolymers. Extrapolating to other phases existing in this system, we believe that the classic diblock copolymer phase diagram [50,51] previously predicted by a GSC model must be significantly revised after the chain rigidity is introduced. This is particularly so for the BCC-stable region [50,51] where $\chi L/a$ is large and the interface width is sharp. Because of a computational limitation, we consider the stability of only the lamellar phase in this work, using a one-dimensional spatial variation; future work that explores full three-dimensional mesostructures is needed to complete the WLC AB diblock copolymer phase diagram and is more demanding in terms of numerical computation.

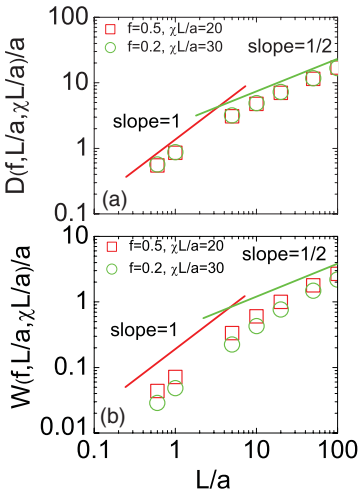

FIG. 6. (Color online) Logarithmic plots of (a) reduced domain size $D(f, L/a, \chi L/a)/a$ and (b) interfacial width $W(f, L/a, \chi L/a)/a$ as functions of chain length L/a. Squares and circles represent systems with fixed parameters ($f = 0.5$, $\chi L/a = 20$) and ($f = 0.2$, $\chi L/a = 30$), respectively. Asymptotic power laws at large and small L/a are indicated by slopes 1/2 and 1, respectively.

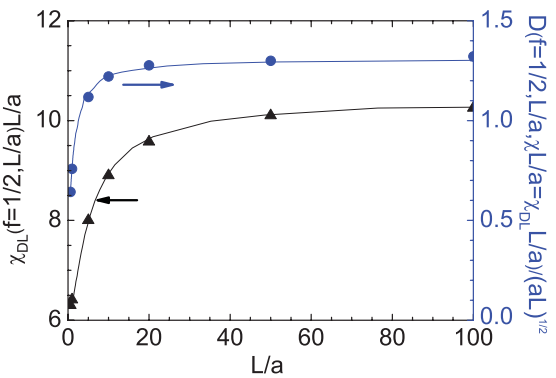

FIG. 7. (Color online) Disorder-lamellar stability boundary $\chi_{\rm DL}(f = 1/2, L/a)L/a$ and the corresponding reduced domain size $D(f = 1/2, L/a, \chi_{\rm DL}L/a)/(aL)^{1/2}$ as functions of the chain rigidity parameter L/a, determined from a wormlike-chain formalism. The triangles and circles represent our numerical results for $\chi_{\rm DL}$ and $D_{\rm DL}$, respectively. The solid curves are plotted by using data read off from Fig. 1 of Matsen's work (for a comparison see Ref. [15]).

In this and related work, there are two basic assumptions made in the study of WLC AB diblock copolymers: the incompressibility condition Eq. (12) and the Flory-Huggins interaction Eq. (1). These two assumptions are identical to those used in studying AB diblock copolymers based on a Gaussian-chain description, where these assumptions can be made by coarse graining over a volume scale of a^3. One important property of a wormlike chain is the angular distribution of a chain segment; strictly speaking, we must include the orientation dependence, beyond the position dependence, in both Eqs. (1) and (12). It is clear that these two conditions are incompatible with the well-known Onsager interaction [52], which also deals with volume packing and alone can produce orientational ordering at the length scale λ or L, whichever is less [18,20,21], when the polymer has a thickness D. A proper procedure for handling the orientation dependence of the incompressibility condition and the Flory-Huggins interaction is desirable and currently unavailable for WLC; the development of such a theory may need the inclusion of a solvent component in the model and yields a model that contains D (or a/D) as an additional parameter. Nevertheless, most current research into understanding WLC AB diblock copolymers adopts these two assumptions [15,23,30].

In this paper we treated the persistence lengths of both AB blocks the same. The formalism can be easily generalized to systems with difference persistence lengths. Of particular recent interest are systems consisting of rod-coil block copolymers, which from experiments appear to have more complicated nanoscale structures [53,54]. The experimental phase diagram for rod-coil block copolymers was constructed by Olsen *et al*. [55–57]. Halperin made an analytical free-energy calculation for rod-coil diblock copolymers theoretically within the scaling approach to study the phase transition between smectic A and smectic C liquid crystals [58]. Shortly thereafter, Williams and Fredrickson extended the theoretical calculations to "hockey puck" micelles, where the rods are packed axially into cylinders [59]. Matsen and Barrett used the self-consistent mean-field theory based on the Semenov-Vasilenko model [19] to study both smectic monolayer and bilayer phases with the assumption that all rods perfectly align along the same orientation [60]. Later, Pryamitsyn and Ganesan performed a similar calculation considering the anisotropic Maier-Saupe interaction and explored the one- and two-dimensional spatial phase diagrams with a variation of the volume fraction of the component coil or rod [61]. Recently, the wormlike-chain model incorporating the anisotropic interaction was used to study the rod-coil diblock copolymers by Song *et al*. [28] on a self-consistent mean-field level. They constructed a lamellar phase diagram consisting of isotropic, nematic, smectic-A, and smectic-C phases. In addition, the lattice-based mean-field simulations [62,63] were also performed for the rod-coil system.

IV. CONCLUSION

We considered a self-consistent-field theory formalism for the calculation of the phase behavior of AB diblock copolymers based on a wormlike-chain model. We focused on the discussion of the disorder-lamellar stability region in this work. We demonstrated that numerical results from the WLC formalism recover those from the Gaussian-chain formalism, for all values of the AB volume ratio f, as long as $L/a \gg 1$ (the flexible limit). Significant modification of the phase stability region needs to be made to the classical phase diagram of AB diblock copolymers when semiflexible polymers are considered. Although the stability boundary shifts, for the wormlike chain model, the phase transition characteristics of the disorder-lamellar stability boundary remain the same as those of flexible chains: second order in the symmetric case ($f = 1/2$) and first order in the asymmetric case ($f \neq 1/2$).

A numerical method, the split-step algorithm, has been developed to handle the computational task of this work. Due to its superior numerical accuracy, the method can be readily used in the study of more complicated mesostructures such as gyroid, hexagonal, and cubic phases.

ACKNOWLEDGMENTS

We thank NSERC for financial support and SHARCNET for computation time. In addition, Y. J. would like to thank Mingge Deng for valuable assistance.

[1] F. S. Bates and G. H. Fredrickson, Phys. Today **52**(2), 32 (1999).
[2] I. W. Hamley, *Developments in Block Copolymer Science and Technology* (Wiley, New York, 2004).
[3] S. F. Edwards, Proc. Phys. Soc. London **85**, 613 (1965).
[4] E. Helfand, J. Chem. Phys. **62**, 999 (1975).
[5] E. Helfand and Y. Tagami, J. Polym. Sci. B **9**, 741 (1971).
[6] E. Helfand and Y. Tagami, J. Chem. Phys. **57**, 1812 (1972).
[7] E. Helfand and A. M. Sapse, J. Chem. Phys. **62**, 1327 (1975).
[8] G. H. Fredrickson, *The Equilibrium Theory of Inhomogeneous Polymers* (Clarendon, Oxford, 2006).
[9] M. W. Matsen, J. Phys. Condens. Matter **14**, R21 (2002).
[10] M. Doi and S. F. Edwards, *The Theory of Polymer Dynamics* (Oxford University Press, New York, 1986).
[11] P. J. Flory, *Principles of Polymer Chemistry* (Cornell University Press, Ithaca, 1953).
[12] O. Kratky and G. Porod, Recl. Trav. Chim. **68**, 1106 (1949).
[13] N. Saito, K. Takahashi, and Y. Yunoki, J. Phys. Soc. Jpn. **22**, 219 (1967).
[14] K. Freed, Adv. Chem. Phys. **22**, 1 (1972).
[15] M. W. Matsen, J. Chem. Phys. **104**, 7758 (1996).
[16] C. Singh, M. Goulian, J. L. Andrea, and G. H. Fredrickson, Macromolecules **27**, 2974 (1994).
[17] P. Friedel, A. John, D. Pospiech, D. Jehnichen, and R. R. Netz, Macromol. Theory Simul. **11**, 785 (2002).
[18] T. Odijk, Macromolecules **19**, 2313 (1986).
[19] A. N. Semenov and S. V. Vasilenko, Zh. Eksp. Teor. Fiz. **90**, 124 (1986).
[20] Z. Y. Chen, Macromolecules **26**, 3419 (1993).

[21] A. Grosberg and A. R. Khokhlov, *Statistical Physics of Macromolecules* (AIP, New York, 1994).
[22] A. Y. Grosberg and D. V. Pachomov, Liq. Cryst. **10**, 539 (1991).
[23] A. J. Liu and G. H. Fredrickson, Macromolecules **26**, 2817 (1993).
[24] S. M. Cui, O. Akcakir, and Z. Y. Chen, Phys. Rev. E **51**, 4548 (1995).
[25] D. Duchs and D. E. Sullivan, J. Phys. Condens. Matter **14**, 12189 (2002).
[26] R. C. Hidalgo, D. E. Sullivan, and J. Z. Y. Chen, J. Phys. Condens. Matter **19**, 376107 (2007).
[27] J. Z. Y. Chen, D. E. Sullivan, and X. Q. Yuan, Macromolecules **40**, 1187 (2007).
[28] W. D. Song, P. Tang, H. D. Zhang, Y. L. Yang, and A. C. Shi, Macromolecules **42**, 6300 (2009).
[29] Y. Jiang and J. Z. Y. Chen, Macromolecules **43**, 10668 (2010).
[30] D. C. Morse and G. H. Fredrickson, Phys. Rev. Lett. **73**, 3235 (1994).
[31] T. W. Burkhardt, J. Phys. A **28**, L629 (1995).
[32] T. W. Burkhardt, J. Phys. A: Math. Gen. **30**, L167 (1997).
[33] D. J. Bicout and T. W. Burkhardt, J. Phys. A: Math. Gen. **34**, 5745 (2001).
[34] J. Z. Y. Chen and D. E. Sullivan, Macromolecules **39**, 7769 (2006).
[35] A. N. Semenov, Eur. Phys. J. E **9**, 353 (2002).
[36] M. G. Deng, Y. Jiang, H. J. Liang, and J. Z. Y. Chen, J. Chem. Phys. **133**, 034902 (2010).
[37] M. G. Deng, Y. Jiang, H. J. Liang, and J. Z. Y. Chen, Macromolecules **43**, 3455 (2010).
[38] L. Lapidus and G. F. Pinder, *Numerical Solution of Partial Differential Equations in Science and Engineering* (Wiley, New York, 1982).
[39] R. A. Fisher and W. K. Bischel, Appl. Phys. Lett. **23**, 661 (1973).
[40] R. A. Fisher and W. K. Bischel, J. Appl. Phys. **46**, 4921 (1975).
[41] W. H. Press, S. A. Teukolsky, W. T. Vetterling, and B. P. Flannary, *Numerical Recipes in C*, 2nd ed. (Cambridge University Press, Cambridge, 1992).
[42] M. W. Matsen and M. Schick, Phys. Rev. Lett. **72**, 2660 (1994).
[43] G. H. Fredrickson, V. Ganesan, and F. Drolet, Macromolecules **35**, 16 (2002).
[44] M. W. Reinsch, J. Math. Phys. **41**, 2434 (2000).
[45] M. Shah and V. Ganesan, J. Chem. Phys. **130**, 054904 (2009).
[46] G. Tzeremes, K. Ø. Rasmussen, T. Lookman, and A. Saxena, Phys. Rev. E **65**, 041806 (2002).
[47] Y. Bohbot-Raviv and Z. G. Wang, Phys. Rev. Lett. **85**, 3428 (2000).
[48] L. Leibler, Macromolecules **13**, 1602 (1980).
[49] F. Schmid and M. Müller, Macromolecules **28**, 8639 (1995).
[50] M. W. Matsen and F. S. Bates, Macromolecules **29**, 1091 (1996).
[51] E. W. Cochran, C. J. Garcia-Cervera, and G. H. Fredrickson, Macromolecules **39**, 2449 (2006).
[52] L. Onsager, Ann. NY Acad. Sci. **51**, 627 (1949).
[53] J. T. Chen, E. L. Thomas, C. K. Ober, and G. P. Mao, Science **273**, 343 (1996).
[54] B. K. Cho, Y. W. Chung, and M. Lee, Macromolecules **38**, 10261 (2005).
[55] B. D. Olsen and R. A. Segalman, Macromolecules **38**, 10127 (2005).
[56] B. D. Olsen and R. A. Segalman, Macromolecules **39**, 7078 (2006).
[57] B. D. Olsen, M. Shah, V. Ganesan, and R. A. Segalman, Macromolecules **41**, 6809 (2008).
[58] A. Halperin, Macromolecules **23**, 2724 (1990).
[59] D. R. M. Williams and G. H. Fredrickson, Macromolecules **25**, 3561 (1992).
[60] M. W. Matsen and C. Barrett, J. Chem. Phys. **109**, 4108 (1998).
[61] V. Pryamitsyn and V. Ganesan, J. Chem. Phys. **120**, 5284 (2004).
[62] W. T. Li and D. Gersappe, Macromolecules **34**, 6783 (2001).
[63] J. Z. Chen, C. X. Zhang, Z. Y. Sun, Y. S. Zheng, and L. J. An, J. Chem. Phys. **124**, 104907 (2006).